12CNIT-2022 - FULL PAPER

A 1D numerical model for a high temperature, shell-side enhanced latent thermal energy store

José Muñoz-Cámara, Hajar Hammou Dahmani, Juan Pedro Solano

Universidad Politécnica de Cartagena, Campus Muralla del Mar, 30202 Cartagena, Spain

Keywords: *Solar Energy; Solar Heat for Industrial Processes (SHIP); PCM*

TOPIC: NUMERICAL SIMULATION AND MODELLING

Abstract

Applications of Solar Heat for Industrial Processes (SHIP) frequently require the coupling of the solar energy source with a thermal energy storage (TES) system, in order to accommodate the solar irradiance dynamics and its fluctuations with the eventually variable heat demand of the process.

The complexity of the physical mechanisms that take place during the phase change process is still a challenge to an accurate modelling while keeping the calculation time low enough to provide fast calculations.

This communication presents a simplified 1D model of a real latent thermal energy storage system with extended surfaces. The model has been validated against a 3D CFD model, providing good results and low calculation times. Preliminary results for a future real application are presented to show the applicability of the model.

1. Introduction

Thermal solar energy has proved its capability to provide clean and cheap thermal energy when solar radiation is available, however, its ability to adapt to the demand when this is not high enough is still a missing link. At the same time, an important fraction of the thermal energy is wasted during summer days. To solve this, latent thermal energy storage systems (LTES) have been proposed.

The use of phase change materials (PCM) in TES systems allows for increasing the amount of energy stored per unit of volume, as well as releasing thermal energy at approximately constant temperature. Conversely, most of PCM currently available for industrial applications present low thermal conductivity. The confinement of the material in a shell and the low motion induced by natural convection during melting and solidification yield very low overall heat transfer coefficients for the TES. This results in poor charging and discharging velocities.

As a solution, two main approaches have been proposed: static and dynamic concepts [1]. Dynamic concepts are typically focused on removing the solidified PCM layer with a low thermal conductivity by using mechanical devices. Static concepts rely on more traditional methods, such as extended surfaces (like fins or honeycombs), to increase the heat exchange area to compensate for the low heat transfer rates.

The use of extended surfaces provides a lower need for maintenance and has been suggested as a reliable method for decreasing the thermal resistance in the shell side of TES systems, where typically the PCM is located.

The prediction of the heat transfer for an industrial-scale system is necessary to a proper sizing of the storage and to design control strategies. There is a wide range of approaches, from analytical models [2] to complete 3D CFD simulations [3]. Analytical models are generally applied to reference problems (e.g., Stefan problem) but are not available to solve complex geometries or to account for buoyancy effects. On the other hand, CFD simulations provide the most reliable description of the heat transfer mechanisms and can describe complex geometries. However, the high computational cost makes not possible to simulate full-scale systems without using supercomputers.

In this work, an intermediate approach is selected, a novel design of shell-side insert is reduced to a 1D model, based on the unsteady heat conduction equation, which is modified to account for the melting and solidification phenomena of the PCM. The model is applied to a global simulation model of a SHIP application, with the aim of proving the energy performance of the system on a yearly basis.

2. Thermal Energy Storage Model

2.1. Geometrical model and simplification

A simplified view of the TES system is depicted in Fig. 1 (a). It consists of a multitube, vertical tank, with six arrays of shell-side inserts per tube. A transverse, 2D view of the insert is depicted in Fig. 1 (b). The 6 cells of the inserts are filled with PCM, and are expected to perform over time with an identical pattern. Additionally, the main temperature gradient is produced in the radial direction. Following the simplification of the cell shown in Fig. 2 centre and left, the heat transfer phenomena can be modelled using the 1D heat conduction equation, considering one cartesian and two radial sub-volumes.

The fin is assumed to be at a uniform temperature, equal to the tube wall temperature, and the deviation from this assumption will be quantified by the fin efficiency. The heat transfer between the fin wall and the PCM is modelled as a convective boundary condition at the PCM boundary using an apparent convective heat transfer coefficient.

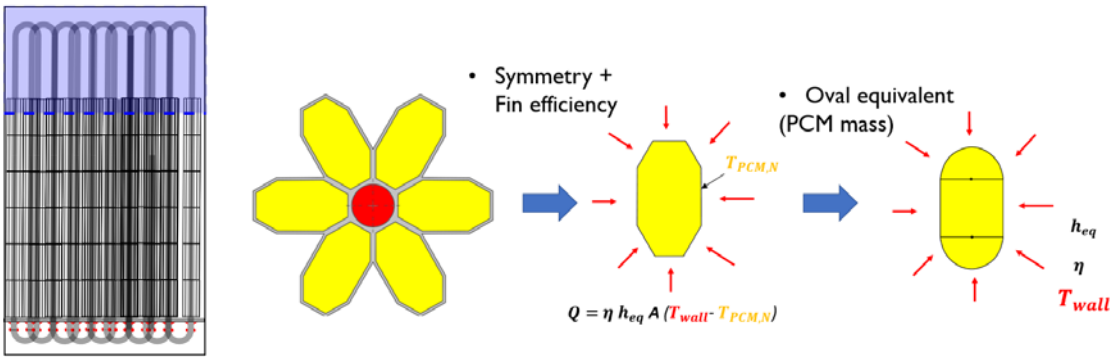

Figure 1. (a) Thermal energy store with shell-side inserts. (b) Geometry simplification for 1D model.

2.2. Numerical model

The simplified geometry is discretized as depicted in Fig. 2:

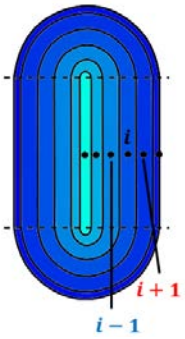

Figure 2. PCM cell volume discretization.

The unsteady heat conduction is applied to each volume is:

$$\rho_i^j \cdot V_i \frac{H_i^{j+1} - H_i^j}{\Delta t} = \frac{\left(k_i^j + k_{i+1}^j\right)}{2} a_n \frac{T_{i+1}^j - T_i^j}{d_n} + \frac{\left(k_i^j + k_{i-1}^j\right)}{2} a_s \frac{T_{i-1}^j - T_i^j}{d_s} \quad (1)$$

Where the indexes i and j refer to the number of the radial element and the time step, respectively. ρ is the PCM density, V the element volume, H the PCM enthalpy in the element, k the PCM thermal conductivity and T the PCM element temperature. a_n and a_s are the areas of the connecting upper and lower adjacent elements, respectively. d_n and d_s are the distance between centres for the upper and lower adjacent elements, respectively. Δt is the time step.

This formulation computes the enthalpy increase [4] directly, so no equivalent specific heat is required. The thermal conductivity, which is used to calculate the heat transfer between two adjacent nodes, is taken as the average of the thermal conductivity calculated at the temperature of the corresponding nodes.

Enthalpy-temperature relation

Once the enthalpy increase on each node has been calculated, this must be translated into an increment on temperature (sensible heat) or liquid fraction (latent heat), depending on the region where the PCM is (solid, liquid or phase transition).

- Solid region: $T_i^j < T_m \rightarrow T_i^{j+1} = T_i^j + {\Delta H_i^j}/{c_p}$; $LF_i^{j+1} = LF_i^j$
- Liquid region: $T_i^j > T_m \rightarrow T_i^{j+1} = T_i^j + {\Delta H_i^j}/{c_p}$; $LF_i^{j+1} = LF_i^j$
- Phase transition: $T_i^j = T_m \rightarrow T_i^{j+1} = T_i^j$; $LF_i^{j+1} = LF_i^j + {\Delta H_i^j}/{H}$

Where T_m is the melting temperature, c_p is the PCM specific heat, LF is the liquid fraction, H is the phase change enthalpy and ΔH is the enthalpy increment between time steps.

Boundary conditions

For the outer node a boundary condition of convection is applied:

$$\rho_i^j \cdot V_i \frac{H_N^{j+1} - H_N^j}{\Delta t} = \frac{\left(k_i^j + k_{i-1}^j\right)}{2} a_s \frac{T_{i-1}^j - T_i^j}{d_s} + \left(\eta \cdot h_{pcm}\right) a_n \left(T_w^j - T_i^j\right) \quad (2)$$

where N is the number of nodes. T_w is the tube wall temperature.

The product of the fin efficiency, η, and the apparent convective heat transfer coefficient, h_{PCM}, must be obtained from experimental or numerical tests, because there are no values in the open literature for such a relatively complex geometry. The complexity is increased if the unsteadiness, natural convection effects and the phase change are considered. In this work, the value of $\eta \cdot h_{PCM}$ will be set to match the results from CFD simulations (see section 2.4).

2.3. Time step and radial mesh analysis

Different numbers of radial nodes and time steps have been studied to analyse the sensitivity of the model to these parameters. To compare the results, the melting times (considered to be the instant when a liquid fraction of a 90 % is achieved) of a reference case (T_w=240 °C, T_{ini}=210 °C) are included in Table 1:

Table 1. Melting times for different time steps and number of nodes.

		Time step		
		0.5 s	0.2 s	0.1 s
Number of radial nodes	5	1072.5 s	1072.4 s	1072.4 s
	10	1136.0 s	1135.6 s	1135.6 s
	20	1144.0 s	1143.8 s	1143.8 s
	30	2376.5 s	1147.0 s	1146.9 s
	40	(No convergence)	1891.6s	1146.4 s
	50	(No convergence)	(No convergence)	**1147.6 s**

The cases with a deviation lower than a 1% from the most precise case (Δt=0.1 s, N=50) are painted in green. Thus, a discretization of 20 nodes and a time step of 0.5 s seems to provide a result good enough while keeping a low computational time.

2.4. Reference CFD model

The CFD model is developed in ANSYS Fluent. One half of a PCM cell is simulated after accounting for the symmetry of the geometry. The model considers the natural convection effects, the heat conduction in the extended surfaces (aluminium alloy) and temperature dependent properties of the thermal salt (with a phase change enthalpy of 104 kJ/kg).

A previous mesh sensitivity analysis was performed to determine the optimum size of the mesh. The outer, upper and lower walls of the insert are considered perfectly insulated. The inner wall temperature of the insert is taken as uniform, and it is time dependent to simulate real charging conditions. The wall temperature (that would replicate the thermal oil temperature at the inlet) is always 5 °C above the average PCM temperature.

Figure 3 shows the contour plot for the liquid fraction (a) and the temperature (b) of the thermal salt in the middle plane of one of the PCM cells for t=100 s.

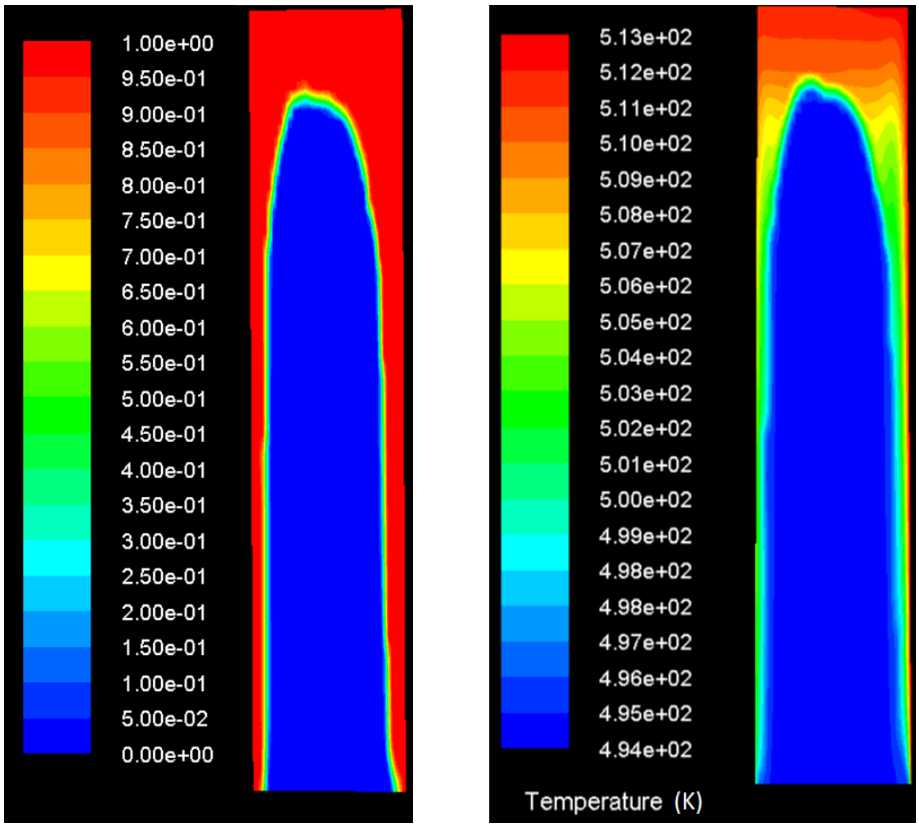

(a) (b)

Figure 3. Liquid fraction (a) and PCM temperature (b) during melting process at time=600 s.

As can be seen, after 10 minutes, a significant amount of the PCM is melted, especially at the upper part of the cell because of the natural convection. The behaviour is then no one-dimensional, there is a significant difference in the thickness of the melted region if the top and bottom sections are compared. This is caused by the growth of the boundary layer along the insert length.

In addition, there is no symmetry because the PCM closer to the tube wall (right side) is absorbing heat at a higher rate. However, despite the difference, it must be highlighted that the insert (fins) is quite effective at distributing the heat around the PCM. The thickness of the melted region at the position which is furthest to the tube wall (left side) is significant when compared to the closest position (right (side).

3. Results

3.1. Model calibration

The model parameters to be calibrated, the product ($\eta \cdot h_{PCM}$), have been adjusted to match the results provided by a preliminary 3D CFD model developed by UPCT (Universidad Politécnica de Cartagena). In the following figures, the results given by the CFD model and the simplified model are compared.

The value ($\eta \cdot h_{PCM}$)=300 W/(m^{2}K) provides good results as can be seen in Figs. 3 and 4, where the evolution of the liquid fraction and the heat wall are compared for the CFD model and the 1D model, for both charging and discharging processes.

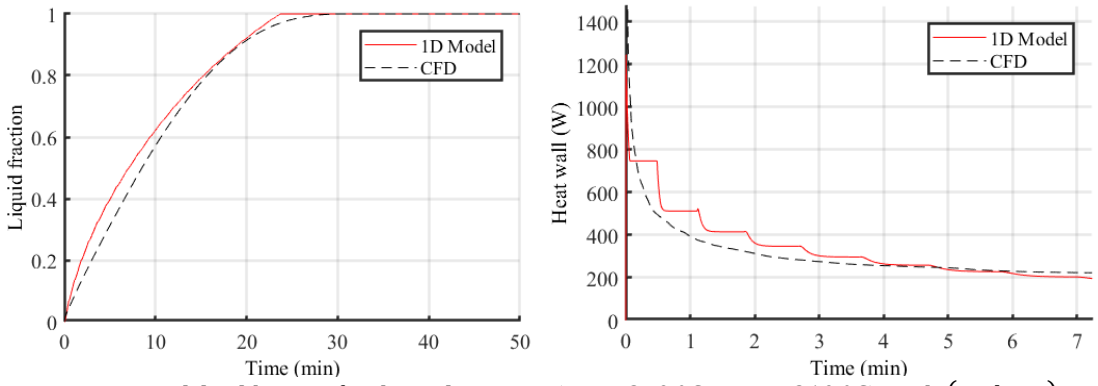

Figure 4. Model calibration for the melting case ($T_w = 240\ °C$, $T_{ini} = 210\ °C$), with $(\eta \cdot h_{pcm}) = 300\ W/(m^2K)$.

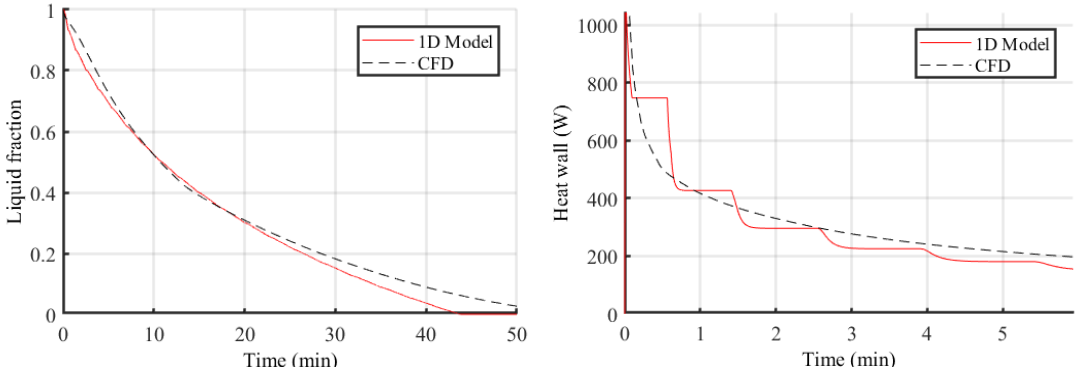

Figure 5. Model calibration for the solidification case ($T_w = 204\ °C$, $T_{ini} = 234\ °C$), with $(\eta \cdot h_{pcm}) = 300\ W/(m^2K)$.

3.2. Axial discretization

While the model does not account for the axial heat conduction, it is expectable that the HTF temperature variation along the tubes could have a relevant effect on the PCM temperature distribution from the inlet to the outlet, and, consequently, on the heat transferred.

In order to determine the optimum number of axial sectors to be modelled, the whole storage unit (it includes 305 inserts) is divided into a different number of axial sectors, from 1 to 8. It is important to remark that these sectors do not represent physically separated modules, they are just a discretization of the storage unit to approximate the effect of the temperature variation along the tube.

The table includes the melting time (*LF*>0.9) and the liquid fraction obtained for these cases:

Table 2. Study of the effect of the number of axial sectors on the melting time.

Number of axial sectors	Melting time (min) [LF>0.9]	LF [time=60 min]
1	97.68	0.5539
2	99.47	0.6143
4	95.20	0.6105
6	95.42	0.6175
8	**95.24**	**0.6157**

As can be seen, a number of axial sections equals to 6 provides a deviation lower than a 1% in comparison to the most accurate case (8 sections).

3.3. Application to a full-size heat storage unit

A full-sized system is considered with 1 tonne of thermal salts (corresponding to 300 inserts) and Therminol 59 as working fluid.

It is expected that the outlet oil temperature is almost the same as the PCM temperature due to the large heat exchange surface area PCM – oil. However, one point of concern is that the oil temperature could be significantly different in response to a sudden change in the power demanded.

A simulation has been performed with the 1D model, starting from the charging process, with a thermal power of 0.5 kW and PCM temperature of 200 ºC. The inlet temperature of the oil is selected to ensure a constant power release.

The power release goes from 0.5 kW (charge) to 7 kW (discharge) when the oil temperature at the outlet reaches 207.5 °C as shown Fig. 5. This sudden change in power demand recreates the start of an absorption chiller. The two different thermal demands are kept constant during the corresponding time interval.

Figure 5 shows the evolution of the average PCM temperature and the inlet ant outlet oil temperatures. As can be seen, after the sudden change in power, after around 4.3 hours, the outlet oil temperature is still quite close to the PCM temperature, and it can be used as a good approximation for control purposes.

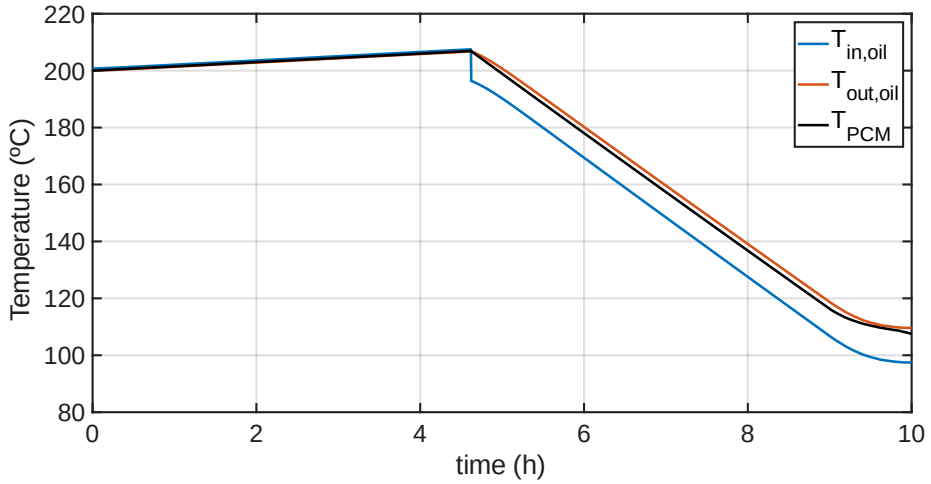

Figure 5. Temperature evolution charge/discharge.

4. Conclusions and Future developments

The main conclusions can be extracted:

- A simplified 1D model has been developed as an approach to solve the heat transfer behaviour of a inserts with a typical 3D flow.
- The model parameters have been successfully calibrated by using a reduce number of CFD simulations.

- Simulation results show that there are no sudden changes in the outlet temperature of the oil when thermal demand changes, making the control easier because the average PCM temperature can be assumed as equal to the outlet oil temperature.

Some developments that are considered to be implemented once experimental results for the whole heat storage unit are available are:

- Effect of the spacings (PCM) between inserts.
- Effect of contact resistance between inserts and the heat transfer fluid tube.
- Heat transfer between adjacent cells. The current model assumes that there is no heat transfer between adjacent PCM inserts.

Acknowledgements

This project has received funding from the European Union's Horizon 2020 research and innovation programme under agreement Nº 884411. This work reflects only the author's view so the Agency is not responsible for any use that may be made of the information it includes.

References

[1] L. Cabeza, L. & N. S. Tay, High-temperature thermal storage systems using phase change materials, 2017.
[2] A. S. Fleischer, Thermal Energy Storage using Phase Change Materials, 2015.
[3] N.H.S.Tay, F.Bruno & M.Belusko, Experimental validation of a CFD model for tubes in a phase change thermal energy storage system, International Journal of Heat and Mass Transfer, 2012.
[4] L. Cabeza, Advances in Thermal Energy Storage Systems, 2015.